Electronic Supplementary Material (ESI) for Journal of Materials Chemistry A.

Supplementary Materials

High-Performance Battery-Supercapacitor Hybrid Device and Electrocatalytic Oxygen Evolution Reaction Based on $NiCo_{2-x}Mn_xO_4$@Ni-MOF Ternary Metal Oxide Core-Shell Structures

*Suprimkumar D. Dhas[1], Avinash C. Mendhe[1], Pragati N. Thonge[1,2], Amar M. Patil[3], Youngsu Kim[1], Daewon Kim[1]**

[1]Department of Electronic Engineering, Institute for Wearable Convergence Electronics, Kyung Hee University, 1732 Deogyeong-daero, Giheung-gu, Yongin 17104, Republic of Korea

[2]Department of Botany, Punyashlok Ahilyadevi Holkar, Solapur University, Solapur, Maharashtra 416 004, India

[3]Energy Conversion Engineering Laboratory, Institute of Regional Innovation (IRI), Hirosaki University, Japan

*Corresponding author: **Professor Daewon Kim**

Email address: daewon@khu.ac.kr

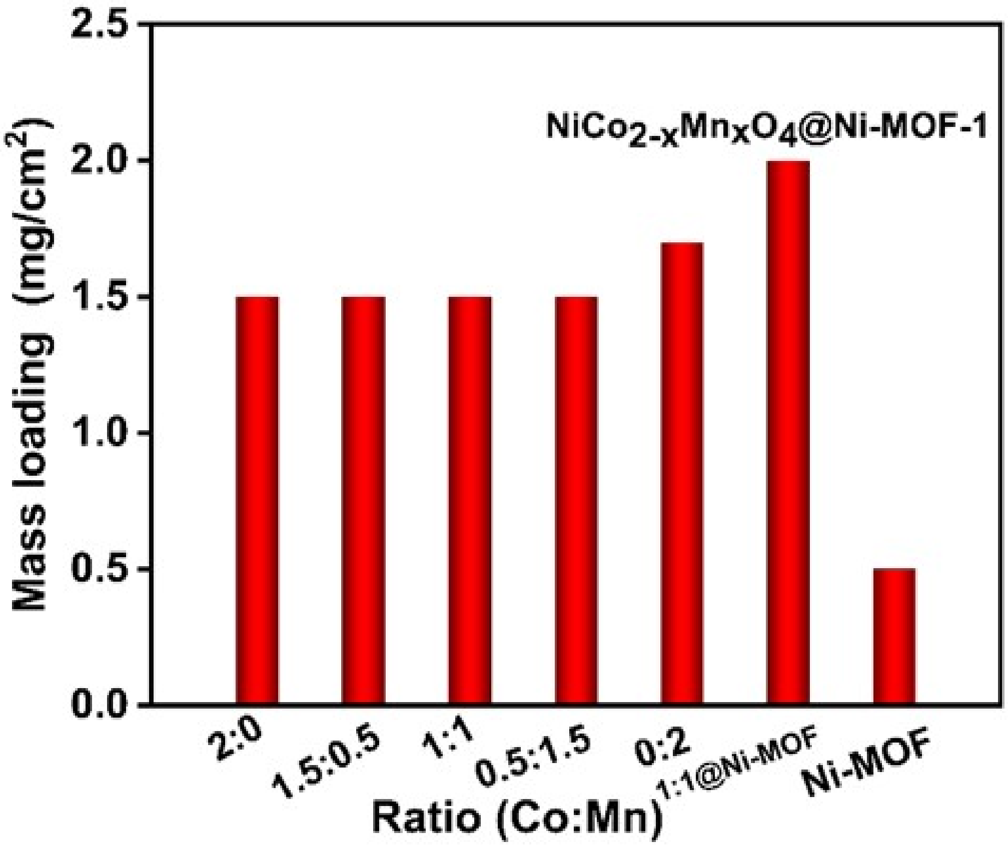

Fig. S1: Bar chart of the mass loading of each $NiCo_{2-x}Mn_xO_4$-based materials

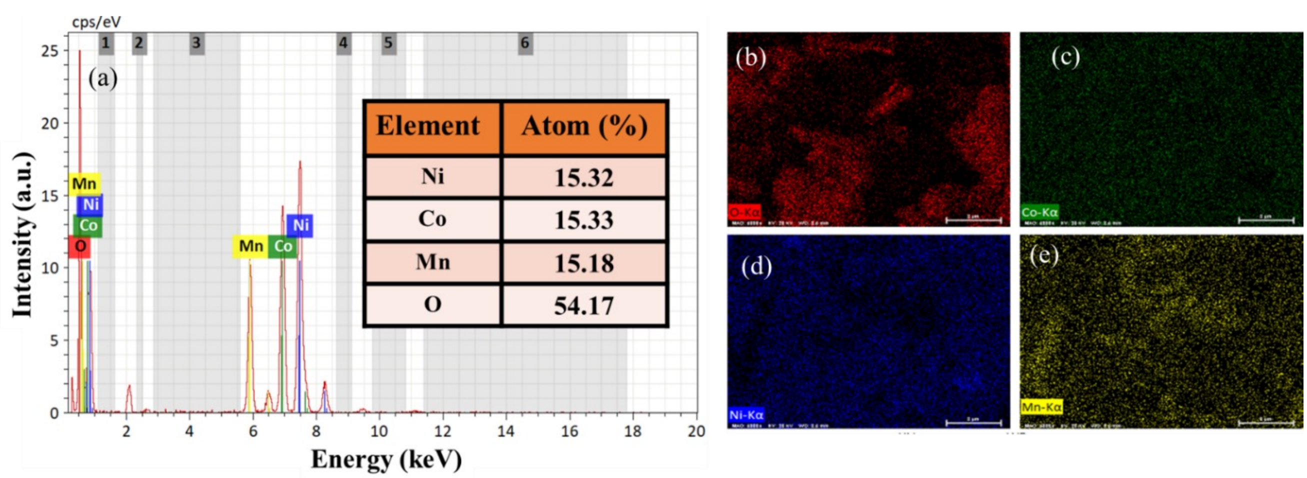

Fig. S2: (a) EDS spectra $NiCo_{2-x}Mn_xO_4$-1 and corresponding element mapping (b) O, (c) Co, (d) Ni, (e) Mn.

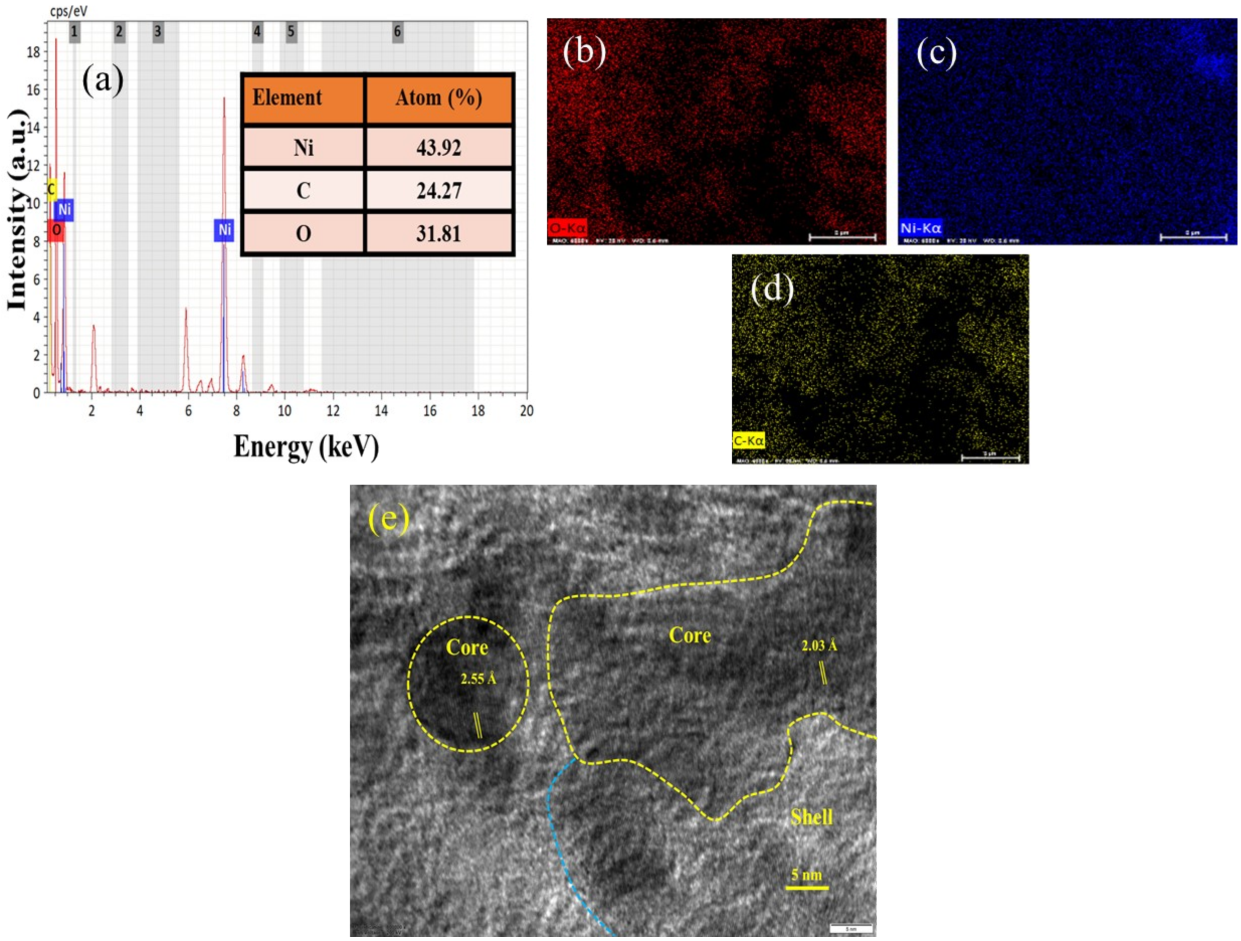

Fig. S3: (a) EDS spectra Ni-MOF and corresponding element mapping (b) O, (c) Ni, (d) C and (e) HR-TEM images of $NiCo_{2-x}Mn_xO_4$@Ni-MOF-1 electrode.

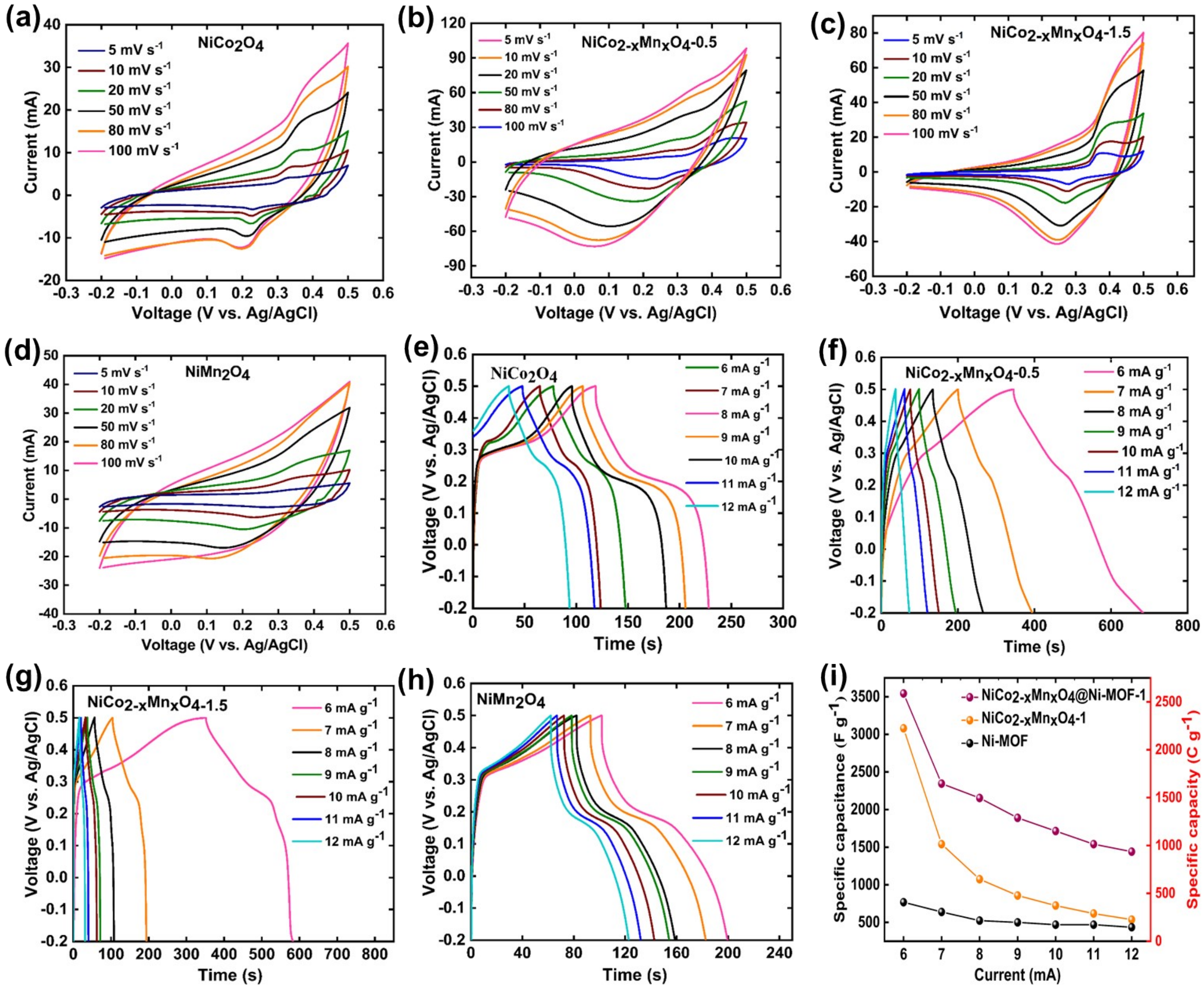

Fig. S4: CV curves of (a) $NiCo_2O_4$, (b) $NiCo_{2-x}Mn_xO_4$-0.5 (c) $NiCo_{2-x}Mn_xO_4$-1.5 and (d) $NiMn_2O_4$, electrodes at various scan rate 5-100 mV/s. GCD curves of (e) $NiCo_2O_4$, (f) $NiCo_{2-x}Mn_xO_4$-0.5 (g) $NiCo_{2-x}Mn_xO_4$-1.5 and (h) $NiMn_2O_4$, electrodes at various current densities. (i) Specific capacitance/capacity vs current densities.

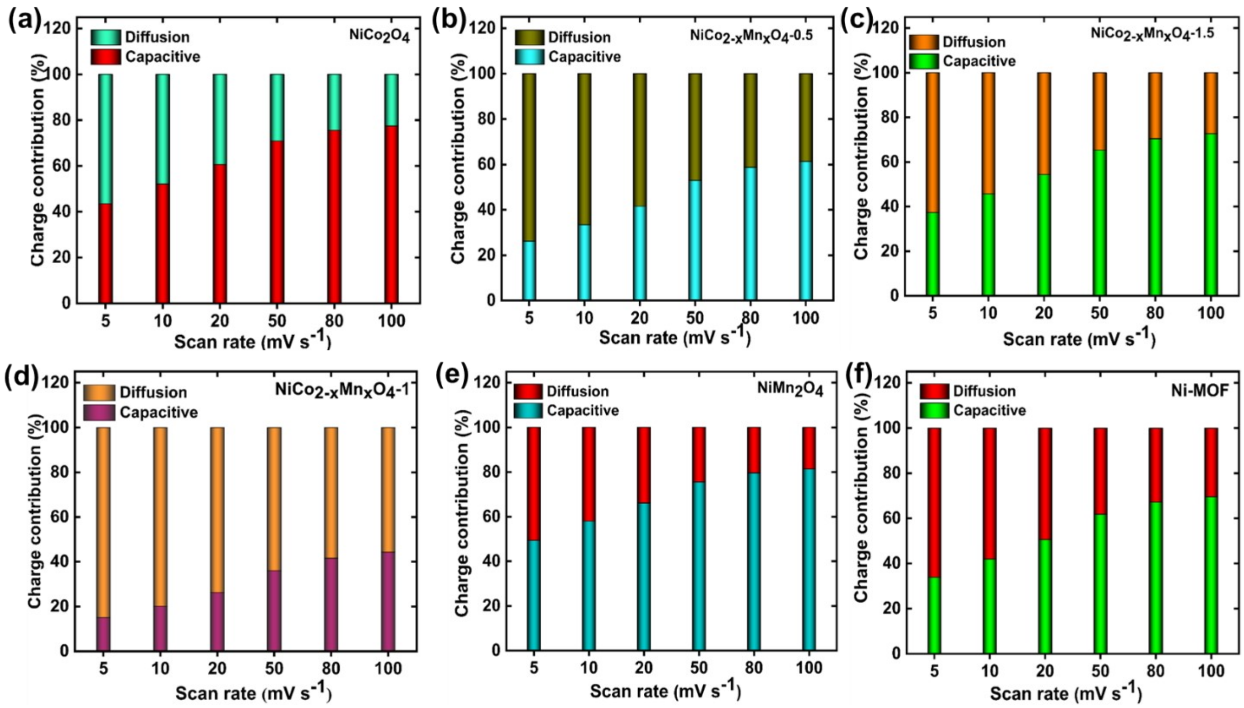

Fig. S5: Capacitive and diffusion-current contributions of (a) $NiCo_2O_4$, (b) $NiCo_{2-x}Mn_xO_4$-0.5 (c) $NiCo_{2-x}Mn_xO_4$-1.5, (d) $NiCo_{2-x}Mn_xO_4$-1, (d) $NiMn_2O_4$ and (f) pristine Ni-MOF electrodes at various scan rates.

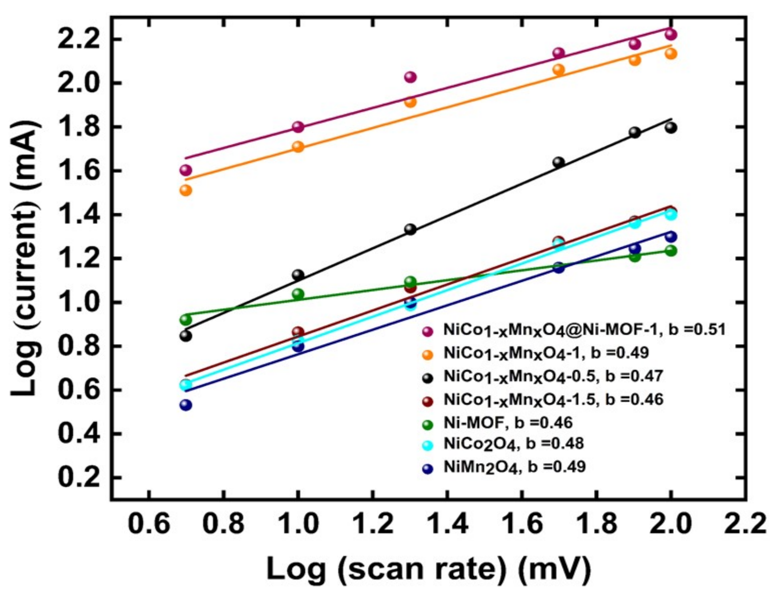

Fig. S6: The b-value determination of the peak anodic currents of $NiCo_{2-x}Mn_xO_4$-based electrodes.

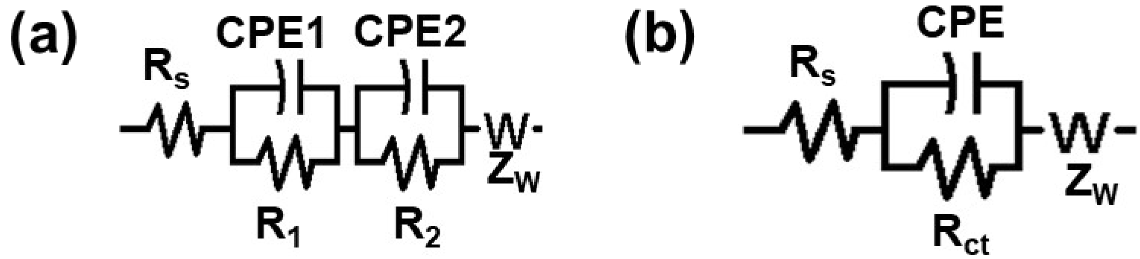

Fig. S7: The equivalent circuit fitted with (a) $NiCo_{2-x}Mn_xO_4$-1, $NiCo_{2-x}Mn_xO_4$-0.5 and (b) $NiCo_{2-x}Mn_xO_4$-1.5, Ni-MOF, $NiCo_2O_4$ and $NiMn_2O_4$ electrodes.

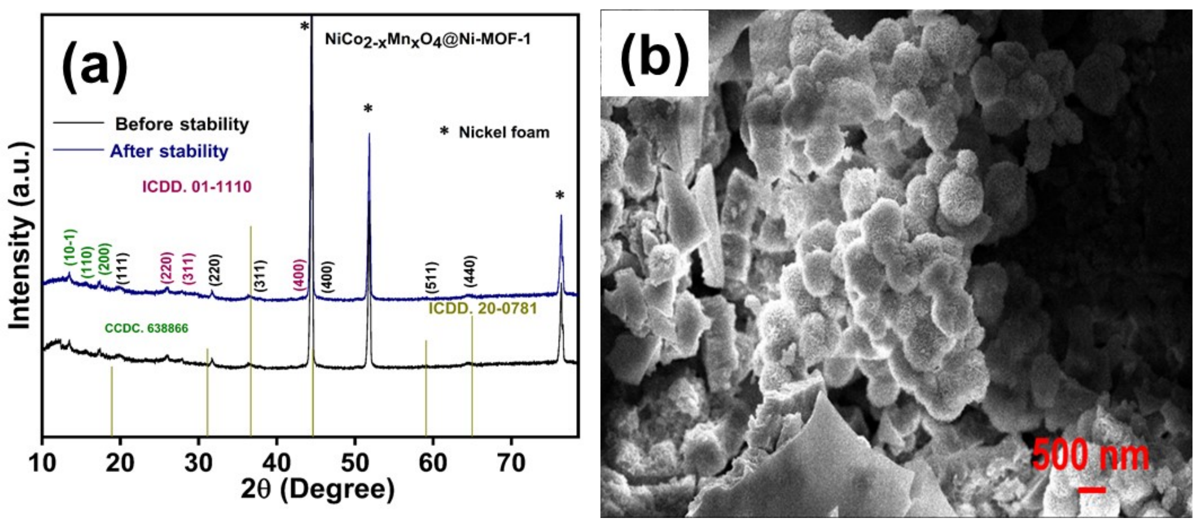

Fig. S8: (a) XRD patterns before and after stability of $NiCo_{2-x}Mn_xO_4$@Ni-MOF-1 and (b) FE-SEM image after stability of $NiCo_{2-x}Mn_xO_4$@Ni-MOF-1 electrode.

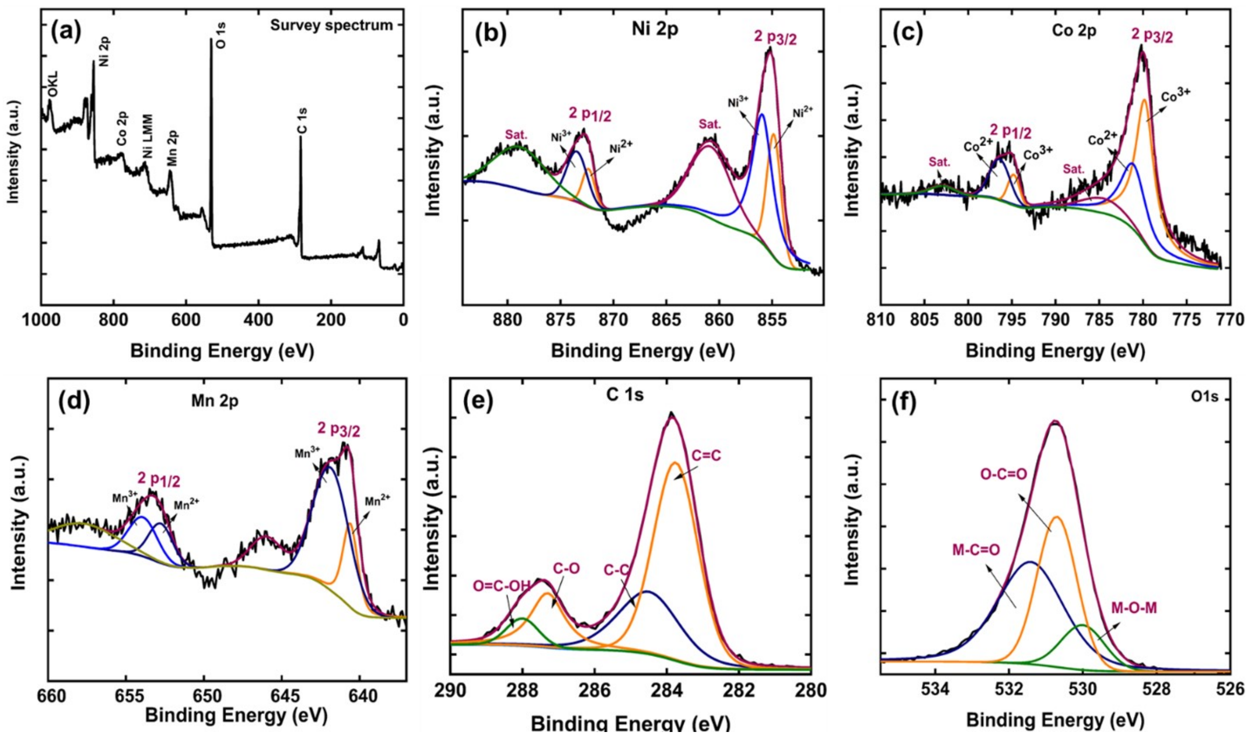

Fig. S9: (a) XPS survey spectrum, after stability of $NiCo_{2-x}Mn_xO_4$@Ni-MOF-1, high-resolution XPS spectra of (b) Ni 2p, (c) Co 2p, (d) Mn 2p, (e) C 1s and (f) O 1s of the after stability of $NiCo_{2-x}Mn_xO_4$@Ni-MOF-1.

Sr. No.	Material based on Ni, Co, Mn, oxides	Method of preparation	Morphology	Electrolyte	Specific capacitance Cs (F/g)	Retention % After Cycles	Ref.
1.	$NiCo_2O_4$@Ni-MOF	Hydrothermal	Nanowires	2 M KOH	208.8 mAh/g (2 mA/cm^2)	-	ACS Appl. Mater. Interfaces 2019, 11, 41, 37675–37684
2.	$NiCo_2O_4$/rGO	Ultrasonic spraying	laminated structure	2 M KOH	871 (1 A/g)	134/30000	J. mater. sci. technol. 99 (2022) 260–269
3.	$NiCo_2O_4$@MnO_2	Electrodepositio n	nanosheets	1 M KOH	913.6 (0.5 A/g)	87.1/3000	J. Mater. Chem. A, 2014,2, 4795-4802
4.	CQD/$NiCo_2O_4$	reflux	sphere	2 M KOH	856 (1 A/g)	98.7/ 10000	J. Mater. Chem. A. 3 (2015) 866–877.
5.	CNT/$NiCo_2O_4$	Electrodepositio n	Nanosheets	6 M KOH	695 (1 A/g)	91/1500	J. Mater. Chem. A, 2017,5, 5886-5894
6.	C@$NiCo_2O_4$	Hydrothermal	microsphere	6 M KOH	404 (1 A/g)	87.1/ 1000	J. Alloys Compd.749, 2018, 305-312
7.	$NiCo_2O_4$@Ni foam	Combustion	honeycomb-like	2 M KOH	646.6 (1 A/g)	96.5/ 3000	Electrochim. Acta 224 (2017) 378–385
8.	$NiCo_2O_4$-ECN	Hydrothermal	Nanoflowers	6 M KOH	596.8 (2 A/g)	97/3100	Electrochim. Acta 1 (2017), 288-295
9.	MWCNT/GO/$NiCo_2O_4$	Hydrothermal	Nanocrystalli ne	6 M KOH	707 (2.5 A/g)	88/5000	J. Alloys Compd,765 (2018), 369-379
10.	$NiCo_2O_4$@rGO	Hydrothermal	nanoneedles	2 M KOH	1427 (8 A/g)	83.8/10000	J. Mater. Chem. A, 2018,6, 22106-22114
11.	CNF@ $NiCo_2O$	Co-precipitation	Nanosheets	2 M KOH	902 (2 A/g)	96.4/2400	Sci. Rep. 3 (1) (2013) 1470.
12.	$NiMn_2O_4$@rGO	Hydrothermal	nanoneedless	6 M KOH	882 (1 A/g)	93.8/5000	Environ. Sci.: Nano, 2020,7, 198-209
13.	PANI- $NiMn_2O_4$	Combustion	Nanospheres	1 M KOH	442	96/1000	Mater. Sci. Eng. B. 294 (2023) 116553
14.	$NiMn_2O_4$/3DPNG	In-situ	Nanocrystals	6 mol/L KOH	1308.2	91.6 %/ 10000	Appl. Surf. Sci. 507, 2020, 145065
15.	$NiCo_2O_4$@ $NiMn_2O_4$	Hydrothermal	nanoneedle arrays	3 M KOH	539.2	93/5000	Ceram. Int.45, 2019, 16904-16910
16.	$CoFe_2O_4$@ $NiMn_2O_4$	Hydrothermal	Nanospheres	1 M KOH	353.6 mAh/g	88.4/10000	J. Alloys Compd. 959, 2023, 170483
	[GNMOP]-[GNMO]-	Hydrothermal	Quasi-		[757] – [436.6] –		Electrochim. Acta

	[NMO]		spherical-sheet		[194]		216, 2016, 386-396
18.	$FeVO_4$ || $NiMn_2O_4$	Combustion	Polyhedral shape	1 M Na_2SO_4	202	91/15000	RSC Advances. 5 (2015) 27649–27656.
19.	$NiMn_2O_4$ @CoS	Hydrothermal	Nano-flakes	1 M KOH	1751	94/5000	ACS Sustainable Chem. Eng. 2018, 6, 12, 16933–16940
20.	$NiCo_{2-x}Mn_xO_4$@Ni-MOF-1	Hydrothermal	Nanoflowers	2 M KOH	3543	93.7/15000	**This Work**

Table S1: Capacitive performance comparison of some nickel, cobalt, manganese based metal oxides and Ni-MOF based electrodes.

The possible reaction mechanism for OER over $NiCo_{2-x}Mn_xO_4$-based electrode:

Hydroxide ion adsorption:

$$NiCo_{2-x}Mn_xO_4 + OH^- \rightarrow NiCo_{2-x}Mn_xO_4\text{-}OH + e^- \quad (1)$$

Oxidation to oxide species:

$$NiCo_{2-x}Mn_xO_4\text{-}OH + e^- \rightarrow NiCo_{2-x}Mn_xO_4\text{-}O + H^+ + e^- \quad (2)$$

Formation of peroxide intermediate:

$$NiCo_{2-x}Mn_xO_4\text{-}O + OH^- \rightarrow NiCo_{2-x}Mn_xO_4\text{-}OOH + e^- \quad (3)$$

Formation and release of oxygen:

$$NiCo_{2-x}Mn_xO_4\text{-}OOH + OH^- \rightarrow NiCo_{2-x}Mn_xO_4 + O_2 \quad H_2O + e^- \quad (4)$$

This proposed mechanism highlights the steps involved in the OER process on a $NiCo_{2-x}Mn_xO_4$-based electrocatalyst, emphasizing the role of each component in facilitating the reaction.

Sr. No.	Catalyst	Overpotential (η) (mV) @ 10 mA cm^{-2}	Tafel slope (mV dec^{-1})	Mass-based specific activity at η = 0.35 V (A g^{-1})
1.	$NiMn_2O_4$	662 ± 9	298.3 ± 0.001	0.93
2.	$NiCo_2O_4$	628 ± 7	272.3 ± 0.008	1.2
3.	$NiCo_{2-x}Mn_xO_4$-1.5	542 ± 6	265.9 ± 0.00514	1.3
4.	RuO_2	467 ± 6	224.4 ± 0.009	3.5
5.	$NiCo_{2-x}Mn_xO_4$-0.5	456 ± 7	189.4 ± 0.0022	2.1
6.	$NiCo_{2-x}Mn_xO_4$-1	393 ± 6	178.1 ± 0.009	5.8
7.	$NiCo_{2-x}Mn_xO_4$@Ni-MOF-1	296 ± 5	131 ± 0.001	8.4

Table S2: Comparative summarized data such as catalyst used, overpotential, Tafel slope with error bar and mass-based specific activity at η = 0.35 V.

Sr. No.	Catalyst	Tafel slope (mV dec^{-1})	Overpotential (mV) @ 10 mA cm^{-2}	Ref.
1.	NiCo-LDH/NiCoPi	73	300	GEE 9 (2024) 1151e1158
2.	NiCo-LDH	123	410	J. Colloid Interface Sci. 604 (2021) 832–843
3.	$Ni_{0.77}Rh_{0.23}O_y$	53.7	310	J. Alloys Compd. 836 (2020) 155309
4.	$NiCoO_2$/CNTs	156	460	Electrochim. Acta. 252 (2017) 338–349
5.	$NiCoO_2$@CFP	57	303	Electrochim. Acta. 174 (2019) 246–253
6.	$NiCoO_x$	N/A	420	J. Mater. Chem. A, 2021, 9, 8576-8585
7.	Ir-doped $NiCo_2O_4$	71	340	Applied Catalysis A, General 626 (2021) 118377
8.	PtCoNi/GNR	76	350	J. Mater. Chem. A, 2020, 8, 17691–17705
9.	Co_3O_4-$NiCo_2O_4$/N-rGO	124	390	Energy and Fuels 2021, 35, 4550.
10.	$NiCo_2O_4$/NCNTs/NiCo	89	350	Chem. Eng. J. 2021, 408, 127814.
11.	$NiCo_2O_4$/CoNC-NS	90.8	352	Int. J. Hydrogen Energy 2023, 48, 13452.
12.	NiCo-LDH	64	307	Carbon 110 (2019) 1e7
13.	Co_3O_4-350°C	55	447	ChemistrySelect 2019, 4, 1131.
14.	$CoNi_{20}$-MOFNs@MX	61.6	379	ChemNanoMat., 2021, 7, 539.
15.	$NiCo_2O_4(CH_3OH)$	45.7	380	ChemElectroChem 2019, 6, 4429.
16.	1% P-$NiCo_2O_4$	95	370	Nanomaterials 2020, 10, 1.
17.	$Ni_{0.75}Cu_{0.25}Co_2O_4$/GF	119	509	Appl. Catal. B Environ. 2021, 291, 120065.
18.	$NiCo_2O_4$	94.63	400	RSC Adv.,2023,13,23547
19.	$NiCo_2O_4$/MXene	64.63	360	ChemCatChem 2024,16, e2023012
20.	$NiCo_{2-x}Mn_xO_4$@Ni-MOF-1	131	296	**This Work**

Table S3: Comparison of OER performance Ni, Mn, Co, oxide based electrocatalysts in alkaline media with recently reported works.